

# **HERD TECHNICAL AND FINANCING FEASIBILITY & WORK PLAN**



# CONTENTS

---

<b>1</b>	<b>trigger system</b>	<b>1</b>
1.1	baseline design	1
1.2	work plan	1
<b>2</b>	<b>crystal array</b>	<b>3</b>
2.1	baseline design	3
2.2	work plan	3
<b>3</b>	<b>IsCMOS camera</b>	<b>5</b>
3.1	baseline design	5
3.2	work plan	5
<b>4</b>	<b>PD system</b>	<b>7</b>
4.1	baseline design	7
4.2	work plan	7
<b>5</b>	<b>FIT</b>	<b>9</b>
5.1	baseline design	9
5.2	work plan	9
<b>6</b>	<b>PSD</b>	<b>11</b>
		<b>iii</b>

**iv** CONTENTS

6.1	PSD Design	11
6.1.1	Scientific motivation	11
6.1.2	Design: the two options	12
6.1.3	The readout and trigger systems	15
6.1.4	Trigger	16
6.1.5	Test results	16
6.2	PSD Work plan	23
	References	25
<b>7</b>	<b>SCD</b>	<b>27</b>
7.1	baseline design	27
7.2	work plan	27
<b>8</b>	<b>TRD</b>	<b>29</b>
8.1	baseline design	29
8.2	work plan	29
<b>9</b>	<b>General structure and thermal</b>	<b>31</b>
9.1	baseline design	31
9.2	work plan	31
<b>10</b>	<b>General electronics and software</b>	<b>33</b>
10.1	baseline design	33
10.2	work plan	33

# CHAPTER 1

---

## TRIGGER SYSTEM

---

this is the trigger chapter.

### 1.1 baseline design

- functions
- working principles, technical approach, main components
- technical specifications, key performance
- resources requirements, device list and external interface
- key technology, technical readiness level, risk analysis
- product matrix

### 1.2 work plan

- work plan(Covering the next two years (phase B and pre-C in ESA/ECSS)), task list and milestone
- product lists and documentation
- target specifications



## CHAPTER 2

---

# CRYSTAL ARRAY

---

this is the crystal array chapter.

### 2.1 baseline design

- functions
- working principles, technical approach, main components
- technical specifications, key performance
- resources requirements, device list and external interface
- key technology, technical readiness level, risk analysis
- product matrix

### 2.2 work plan

- work plan(Covering the next two years (phase B and pre-C in ESA/ECSS)), task list and milestone
- product lists and documentation
- target specifications



## CHAPTER 3

---

# ISCMOS CAMERA

---

this is the IsCMOS chapter.

### 3.1 baseline design

- functions
- working principles, technical approach, main components
- technical specifications, key performance
- resources requirements, device list and external interface
- key technology, technical readiness level, risk analysis
- product matrix

### 3.2 work plan

- work plan(Covering the next two years (phase B and pre-C in ESA/ECSS)), task list and milestone
- product lists and documentation
- target specifications



## CHAPTER 4

---

### PD SYSTEM

---

this is the PD chapter.

#### 4.1 baseline design

- functions
- working principles, technical approach, main components
- technical specifications, key performance
- resources requirements, device list and external interface
- key technology, technical readiness level, risk analysis
- product matrix

#### 4.2 work plan

- work plan(Covering the next two years (phase B and pre-C in ESA/ECSS)), task list and milestone
- product lists and documentation
- target specifications



## CHAPTER 5

---

### FIT

---

this is the FIT chapter.

#### 5.1 baseline design

- functions
- working principles, technical approach, main components
- technical specifications, key performance
- resources requirements, device list and external interface
- key technology, technical readiness level, risk analysis
- product matrix

#### 5.2 work plan

- work plan(Covering the next two years (phase B and pre-C in ESA/ECSS)), task list and milestone
- product lists and documentation
- target specifications



## CHAPTER 6

---

### PSD

---

#### 6.1 PSD Design

##### 6.1.1 Scientific motivation

The main purpose of the Plastic Scintillator Detector (PSD) in HERD is to select in real-time low energy gamma rays by vetoing the low energy charged particles triggering the calorimeter (CALO). The PSD is also designed to identify CR nuclei up to iron by exploiting the energy loss in the interactions, thus complementing the Silicon Charge Detector (SCD) measurements. Electron and proton induced events can be separated by analyzing the shower profiles in the CALO. The discrimination between electron and gamma ray events (both generating electromagnetic showers) can be effectively performed only by using thin and light plastic scintillators. The interaction of gamma rays with the calorimeter may produce *backsplash effect* [1]. A small fraction of secondary particles (mostly 100-1000 keV photons) from the electromagnetic shower created by an high energy photon, travels backwards through the tracker and interacts with the plastic scintillators, where they can release energy by Compton scattering. These signals end up triggering the VETO and thus causing the rejection of events induced by high energy photon interactions. The back-splash due to  $GeV$  photons has an impact on the photon detection efficiency at higher energies ( $> 10 GeV$ ): to give some context, in the DAMPE experiment [2] almost 30% (50%) of gammas are rejected in the energy range  $1 - 100 GeV$  ( $100 GeV - 1 TeV$ ) due to back-splash [3]. Although more important for gamma selection, the back-splash from charged particles can also affect the charge measurement both by worsening the resolution and by

leading to a misidentification of the charge due to the contribution of the back-scattered particles to the energy deposit. The PSD segmentation (bar- and tile-based configurations are under study, see section 6.1.2), together with the absence of high density material (i.e. Tungsten) between the calorimeter and the PSD, the optimization of the geometrical configuration of the PSD, can mitigate such effect. For the bar-based configuration of the DAMPE experiment, a residual misidentified charge rejection due to the back-scattered particles is at a level of 5-10 %, depending on the energy deposited in the calorimeter. In order to minimize the number of unwanted interactions of gamma rays in the PSD and enhancing its capability of detecting charged particles, organic plastic scintillator (relatively low density, good radiation hardness, suitable for large scale production at relatively low cost) represents a good choice to fulfill the PSD requirements. The PSD is also capable of performing charge measurement of the incoming CR particle. Nevertheless, due to the fragmentation effect induced by high Z CR ion interactions in the PSD, HERD adopted a Silicon Charge Detector (see section 7), surrounding all the sub-detectors, whose primary task is to provide the charge measurement of the incident CR.

### 6.1.2 Design: the two options

The PSD is designed to work as anti-coincidence detector and to provide an additional measurement of CR charge. To pursue these goals, PSD main requirements are:

- high detection efficiency for Minimum Ionizing Particles (MIPs),
- very high hermeticity,
- good energy resolution for charge measurement,
- large dynamic range to cope with high intensity scintillation light emission typical of high Z CR ions (up to iron and beyond).

Differently from its predecessor DAMPE, the HERD PSD will surround five sides of the calorimeter, see fig. 6.1a. In this configuration, very important is the hermeticity, a parameter that strongly affects the capability of the detector to discriminate gamma and charged particle events. Geant4-based simulations have been performed to optimize size, positioning and shape of each PSD plane in order to ensure an hermeticity larger than 99.98%. In

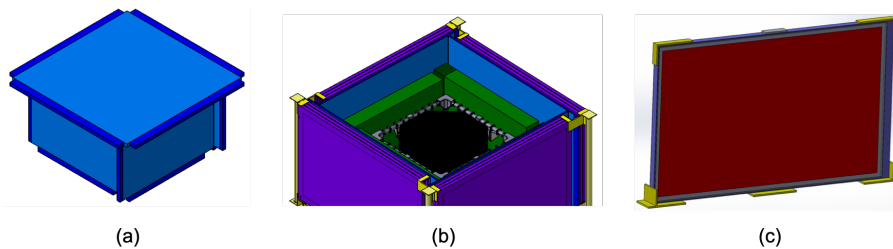


**Figure 6.1** (a) CAD model showing the positioning of the PSD planes. (b) Section of the HERD CAD model showing the interconnection among sub-detectors (assuming the wall sequence from outer to inner : in violet the SCD, in blue the PSD, in green the FIT and in black the CALO). (c) The frame and the anchor points needed to keep the detector first natural frequency above  $\sim 100$  Hz

the current design, the four lateral planes have dimensions of  $164.5\text{ cm} \times 94.3\text{ cm} \times 5\text{ cm}$

and these are positioned in such a way that each plane protrudes over the next one by 10 cm. The top squared plane ( $183\text{ cm} \times 183\text{ cm} \times 5\text{ cm}$ ) protrudes out the sides. Fig. 6.1b shows a cross-section of HERD in which the interconnection among sub-detectors is visible. PSD and SCD have identical dimensions: the mechanical support structure has been designed to ensure that each side of the two sub-detectors can be mounted in one tray.

Currently, two designs are being considered for the PSD: one based on the use of plastic scintillator bars, the other based on tiles. Regardless the PSD configuration, SiPMs have been selected as photosensors (see Sect. 6.1.3) thanks to their intrinsic properties (high detection performance, low weight, compactness, magnetic field insensitivity, suitability for low power applications).

**6.1.2.1 The bar option** Geant4 simulations have been performed in order to optimize the bar shape in terms of detection features, compactness and hermeticity of each PSD plane. According to the simulation predictions, the optimal PSD detection unit is made out of a trapezoidal bar with an angle of  $45^\circ$ . Each bar is read out at the two ends by SiPMs, see fig.6.2. Each PSD plane is composed of two layers of trapezoidal bars perpendicularly

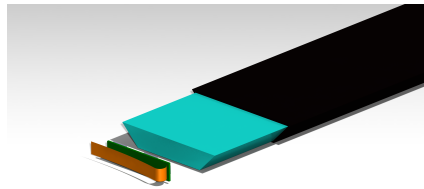


**Figure 6.2** CAD design of the detection unit in the bar PSD concept.

overlapped in order to provide the bi-dimension position reconstruction and therefore instrumental for the SCD and FIT track identification and charge measurement, see fig. 6.3.

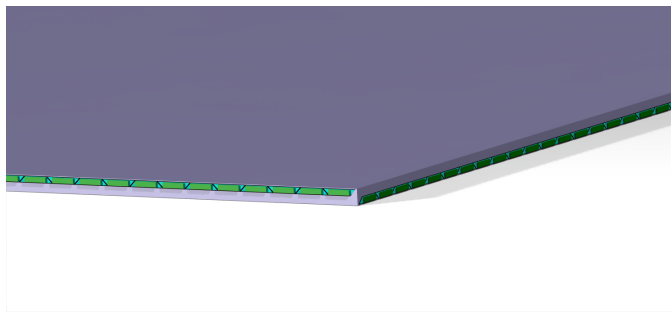


**Figure 6.3** Detail of the PSD concept based on trapezoidal plastic scintillator bars.

The top plane consists of 134 bars, 67 for each layer, of  $174.2\text{ cm} \times 3\text{ cm} \times 0.5\text{ cm}$  dimension. Each lateral plane consists of 99 bars, 61 + 38 bars arranged in the two layers, of  $159\text{ cm} \times 3\text{ cm} \times 0.5\text{ cm}$  dimension for the horizontal bars and  $93.3\text{ cm} \times 3\text{ cm} \times 0.5\text{ cm}$  for the vertical bars. The bars in each PSD plane are housed in a carbon fiber structure, as shown in fig. 6.3. Such structure, along with the corresponding SCD plane, is anchored in the tray in a way that keeps the first natural frequency of the detector above 100 Hz,

see fig. 6.1c. The overall weight of the bar-based PSD option is of about 194 kg. In this evaluation, the weight of electronics and cables are not taken into account.

**6.1.2.2 The tile option** In this concept design, the PSD detection unit is made out of a plastic scintillator tile. This option foresees two layers of tiles for each PSD plane as well. In order to ensure the highest possible hermeticity, the two layers of tiles are staggered, as visible in fig. 6.4. Each tile can be read out by SiPMs placed either on two opposite sides

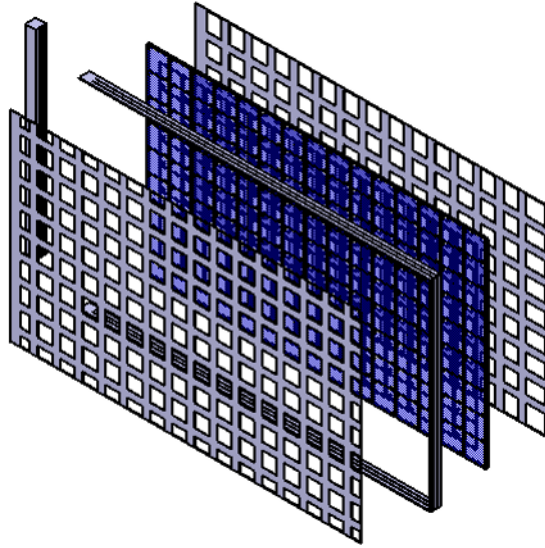


**Figure 6.4** Exploded model of one of the PSD lateral planes made out of staggered tiles.

(see fig. 6.5(a)) or on the surface (see fig. 6.5(b)). For this latter, the SiPMs are mounted on long Printed Circuit Board (PCB) housing 5 to 10 tiles.

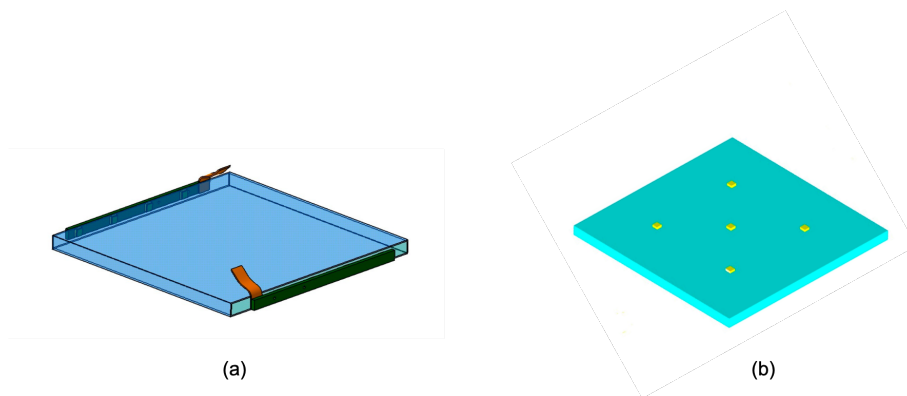


**Figure 6.5** CAD model of a plastic scintillator tile. Left: the option in which the SiPMs are positioned on two opposite sides. Right: the option in which the SiPMs are positioned on the top surface of the tile.

Similarly to the bar PSD concept, the two layers of tiles are housed in a carbon fiber structure, coupled to the corresponding SCD plane and anchored inside the tray in a way

that keeps the first natural frequency of the detector above 100 Hz, see fig. 6.1c and fig. 6.6. The top plane of the PSD consists of 578 tiles with dimensions of  $10\text{ cm} \times 10\text{ cm} \times 0.5\text{ cm}$ ,

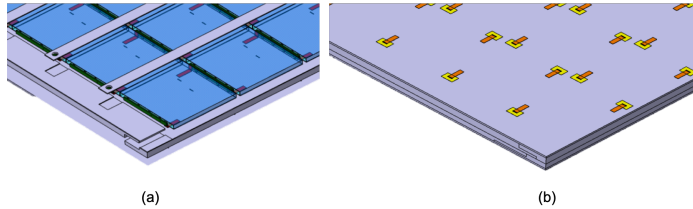


**Figure 6.6** Detail of the PSD concept based on plastic scintillator tiles.

while each side features 284 tiles  $9.3\text{ cm} \times 9.3\text{ cm} \times 0.5\text{ cm}$ . The overall weight of the tile-based PSD option is of about 202 kg. In this evaluation, the weight of electronics and cables are not taken into account.

### 6.1.3 The readout and trigger systems

As reported in the previous sections, SiPMs have been chosen as photosensing technology for reading out the scintillation light in the PSD of HERD. The main characteristics of SiPMs are: excellent photon counting capability, sensitivity to few photons, fast response, low weight, negligible power consumption and insensitivity to magnetic fields. All these features make SiPMs ideal for space applications. The PSD will be designed according to the results obtained by running R&D campaigns on several prototypes based on tile and bar concepts (see section 6.1.2), in which SiPMs from different manufacturers, with different dimensions and cell sizes have been evaluated as well. In order to effectively identify the incident high energy particles through the charge measurement (up to  $Z=26$ ), a good charge resolution is mandatory for the PSD, which means a good resolution in the deposited energy measurement. Therefore, the detector dynamic range should cover more than two decades. This task can be accomplished by SiPMs and different solutions are under study. The chosen SiPM should feature photon detection efficiency (PDE) suitable for a low level trigger logic with a threshold set to  $1/3$  of MIP. Section 6.1.5 reports the main results obtained during the R&D campaign in terms of dynamics and PDE. The Hamamatsu S14160[4] Multi-Pixel Photon Counters (equivalent to SiPMs) performed the best and match almost all the PSD requirements. Two SiPM models have been selected for the realization of the prototype for the test beam.

- (a) device size:  $1.3\text{ mm} \times 1.3\text{ mm}$ , cell size:  $10\mu\text{m}$ ;
- (b) device size:  $3\text{ mm} \times 3\text{ mm}$ , cell size:  $15\mu\text{m}$ .

The smallest SiPMs(a) are intended to be used for the detection of high  $Z$  nuclei, whose interactions produce an higher number of scintillation photons compared to low  $Z$  CR interactions. For the latter and MIP detection, the largest SiPMs (b) are used. Regardless the very promising results obtained, there is room for further improvements, more specifically we shall:

- test SiPMs of type (b) with larger cell size to enhance MIP(and low  $Z$  nuclei) detection capability;
- study the radiation hardness of these devices;

- study the coupling between photosensors and plastic scintillators.

SiPMs designed and developed at Fondazione Bruno Kessler (FBK) [5] are being evaluated as well. The FBK manufacturing process ensures:

- radiation hardness;
- high fill factor (i.e. improved PDE);
- low crosstalk.

After a successfully testing campaign on a handful of prototypes, in Fall 2022 a first official batch of FBK custom SiPMs will be made available for testing the two PSD configurations (tiles and bars). The SiPM analog signal will be read out by a custom ASIC chip ( $\beta$ -chip, see section ??) designed at the Institute of Cosmos Sciences - University of Barcelona (ICCUB, Spain). Even though the  $\beta$ -chip has been originally intended for its use in the Fiber Tracker, it fulfills the requirements of PSD SiPM readout. The  $\beta$ -chip has been designed for low power applications (down to 1 mW per detection channel) and it features a wide dynamic range.

#### 6.1.4 Trigger

As already mentioned, the PSD has the major role of selecting low energy gamma rays by vetoing low energy charged particles. This is of great importance especially at low energies, where the trigger logic FIT+CALO is active: most of the signals in the low energy range are indeed generated by low energy protons.

In the working scenario, multiple signals of PSD detection units (bars or tiles coupled to SiPMs) are read out by *beta-chips*. Each *beta-chip* can be configured to read out multiple of eight channels (8, 16... 128). The *beta-chip* produces a standard output optimized for the charge measurement and a fast digital output which can be used for the trigger logic. The PSD DAQ follows a hierarchical scheme, see fig. 6.7:

1. the SiPM analog signals are read out by the *beta-chips* which implement the lowest level trigger logic (L1) by checking the readout channels over threshold;
2. a group of *beta-chips* is handled by a FPGA (the number is still under evaluation) that implements a medium level trigger logic (L2), by searching for a majority of spatially correlated detection units over threshold;
3. for each PSD plane a central FPGA distributes a high level trigger logic (L3) among the FPGAs handling the *beta-chip* group, to search for a signal correlation with the other sub-detectors.

#### 6.1.5 Test results

An extensive R&D activity involving the two PSD concepts is in progress at Gran Sasso Science Institute(GSSI), at Gran Sasso National Laboratory(LNGS), and in the INFN laboratories of Bari and Pavia. In addition to the characterization tests performed with cosmic rays and  $^{90}\text{Sr}$  radioactive source, the PSD prototypes underwent several beam tests:

- 2018 at PS (Proton Synchrotron) and SPS (Super Proton Synchrotron) facilities at CERN;

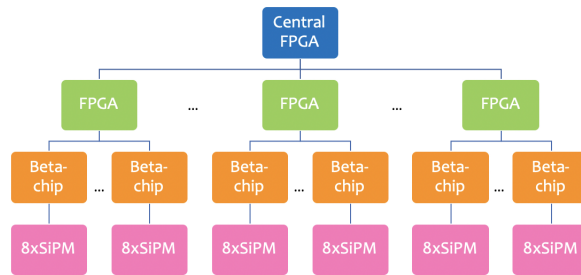


**Figure 6.7** Hierarchical scheme of the PSD DAQ for a single plane

- 2019-2021 at CNAO (National Center for Oncological Hadrontherapy) synchrotron in Pavia, Italy;
- 2021 at PS and SPS facilities at CERN.

**6.1.5.1 The CNAO test beams** The available beams at CNAO for characterization and testing purposes are made out of:

- protons(p) with kinetic energy in the continuous range 60-250 MeV and rate up to  $10^{10}$  p/s;
- carbon(C) ions with kinetic energy in the continuous range 120-400 MeV/u and rate up to  $4 \times 10^8$  C/s.

Given that the particles are not ultrarelativistic,  $\beta < 1$ , a user can test the ion energy loss up to Al.

Both the tile readout approaches (readout on opposite sides and on surface) have been tested (see fig.6.8), in order to study the response of two different SiPM configurations [6].

Figure 6.9 shows the results of the single Hamamatsu SiPM signal compared to the PCB with embedded SiPMs (blue points). Those results are overlapped to the expected values obtained from the MC simulation (red continuous line). This result is a pathway for future tests, e.g. using the carbon beam, to mimic heavier ions and test the quenching saturation effect characteristic of the plastic scintillator materials, according to the Birks' saturation law [7].

**6.1.5.2 The CERN test beams** A first test beam was conducted at CERN in 2018 with the aim at characterizing two single PSD tile prototypes, the first one ( $15\text{ cm} \times 15\text{ cm}$  with a thickness of  $1\text{ cm}$ ) at PS-T10 ( $5\text{ GeV}/c$  particles) and at SPS-H8 ( $20\text{ GeV}/c$  particles) obtaining a very high particle detection efficiency (99.999%) and the second one ( $10\text{ cm} \times 10\text{ cm}$  with a thickness of  $1\text{ cm}$ ) was tested at SPS-H4 with heavy ions ( $330\text{ GeV}/Z$ ) to test the saturation effect in scintillation light production due to the Birks' quenching effect [7]. The results were compared with a MC simulation and published [10, 11].

In 2021 for the first time, scaled prototypes ( $\sim 50\text{ cm} \times 0\text{ cm}$ ) of both PSD concept designs were tested at CERN along with the other HERD sub-detector prototypes, see fig. ???. The tile PSD prototype was made out of a single layer of 20 plastic scintillator tiles organized in an array of  $4 \times 5$  elements (each one of  $10\text{ cm} \times 10\text{ cm} \times 0.5\text{ cm}$  dimensions). The tiles, wrapped with a sheet of Tyvek, were read out by two PCB boards, each one embedding

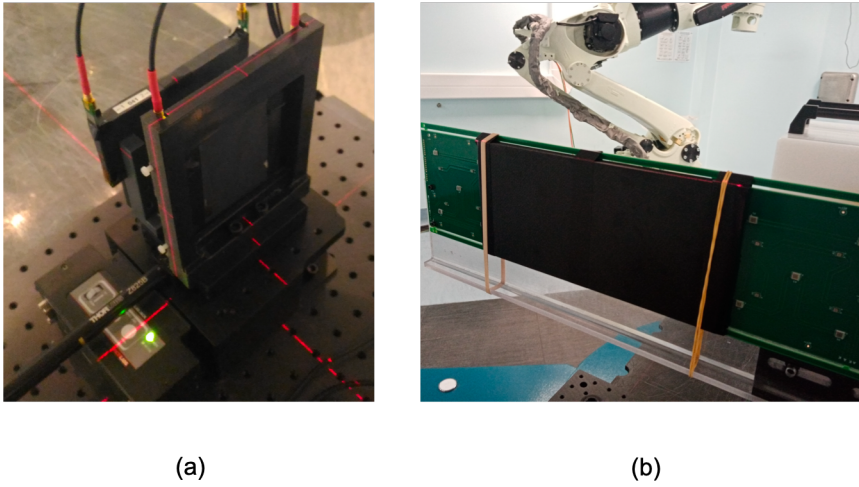


**Figure 6.8** The setup tested at CNAO. LEFT: A  $10\text{ cm} \times 10\text{ cm}$  tile read out at the opposite sides (see fig. 6.5) followed by a tile that acts as trigger. RIGHT: Two  $10\text{ cm} \times 10\text{ cm}$  tiles read out at the surface by using a  $50\text{ cm}$  PCB with embedded SiPMs.

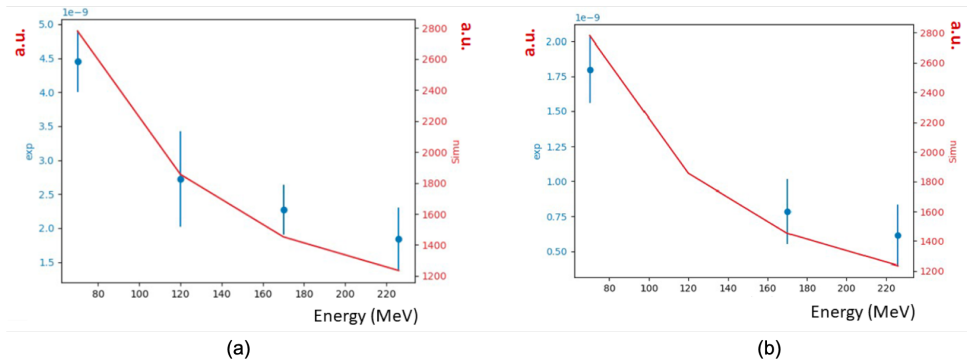


**Figure 6.9** RIGHT: signal generated by an Hamamatsu S12572-010c [8]  $3 \times 3\text{ mm}^2$  with  $10\mu\text{m}$  pitch SiPM. LEFT: signal generated by a PCB board equipped with 3 S12572-050p [9]  $3 \times 3\text{ mm}^2$  with  $50\mu\text{m}$  pitch SiPMs, blue points. The results were obtained by exposing the prototype to a proton beam at different energies. The results of a MC simulation (red continuous line) are reported for comparison.

3 SiPMs in *or-logic*. In the prototype, the two readout options for tiles were adopted. Different SiPMs (MPPC S14160-30050 and S14160-1315) and different materials (BC-404 and BC-408) were used for performance comparison. Both tile and bar prototypes adopted the same read-out system, based on the CAEN Citiroc-based board DT5550W [12]. Figure 6.11 shows two examples of hit maps obtained at PS using the pion beam. The colors and the number shown are the normalized hit rates obtained for lines from A, B and C. The hit is recorded when the signal amplitude is larger than  $1/3$  of the MIP one and event is detected by both the SiPM PCB boards. The right figure shows the hit rate when the beam hits the center of a single tile (tile B1) and the left figure when the beam hits the corner of 4 different tiles (C0,C1,B0 and B1). These maps were produced to study

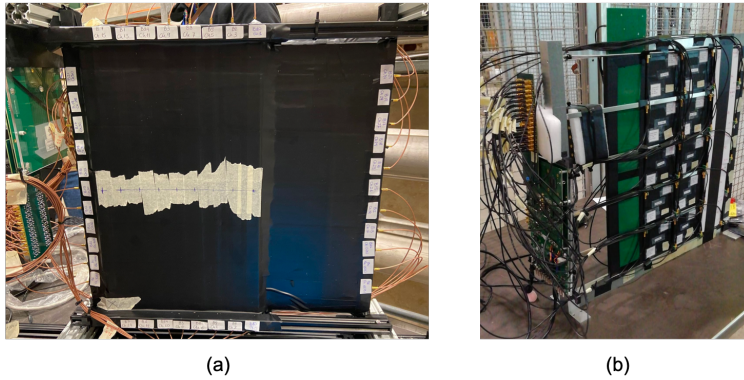


Figure 6.10 LEFT: the bar PSD prototype. RIGHT: the tile PSD prototype.

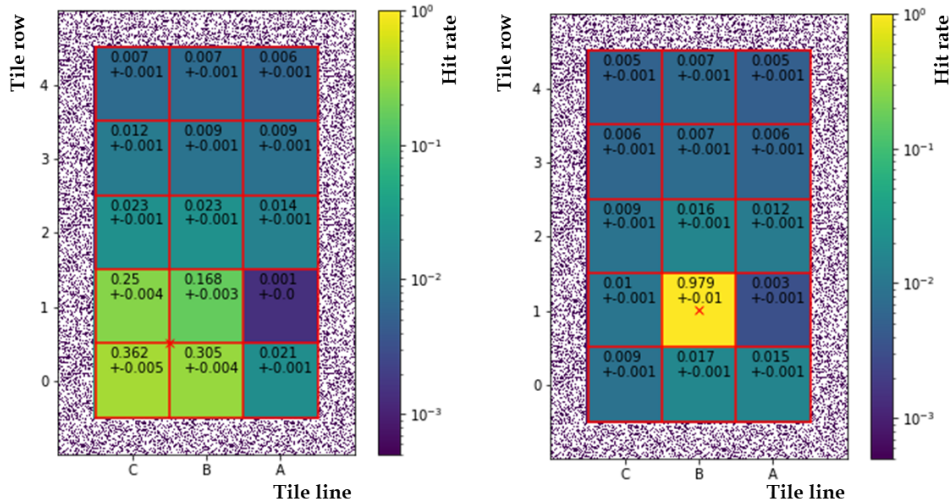
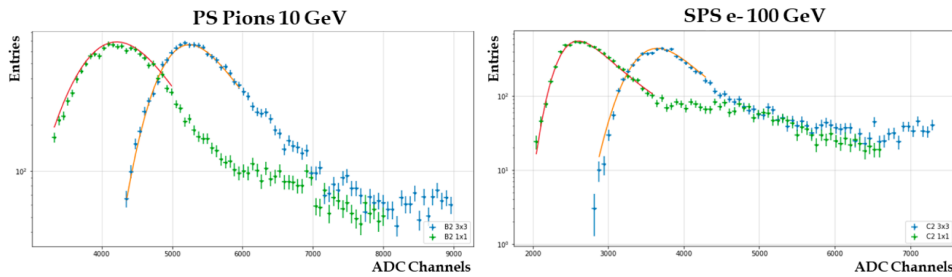


Figure 6.11 Normalized hit rate for the 10 GeV pions beam (at PS). LEFT: the beam is centered at the intersection of the 4 tiles C0, B0, C1, B1. RIGHT: the beam impinges in the center of tile B1. The hits are recorded when the signal amplitude is larger than 1/3 of a MIP signal and it is simultaneously detected and generated in the two PCB boards.

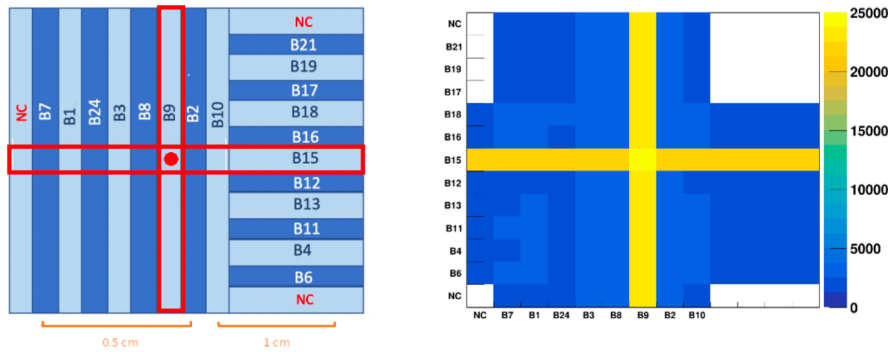
the noise contamination in tiles neighboring the fired one. This value, as shown, is about 1% in the neighbour tiles of the fired one (probably due to beam contamination), while it is less than 0.5% in the further ones.

Fig. 6.12 shows the signals acquired for MIPs in tile B1 (Figure 6.11right can be used as reference). These measurements were carried out to study the uniformity of the response in the same tile when a particle hits different positions. The other PSD prototype, for the CERN beam test campaign, was made out of 50 cm long trapezoidal shaped bars with 45°angle. Two thickness values (1 cm and 0.5 cm) and 2 scintillator materials (BC-404 [13] and EJ-204 [14]) were used. All the bars were read out by means of PCBs housing 2 MPPC S14160-3050 in *or-logic* for each side of the bar. The prototype consisted of 2 overlapped layers of bars, respectively arranged along X and Y axes. With this configuration, the beam position is identified by the intersection of two bars. Fig. 6.13b shows



**Figure 6.12** Signal acquired in tile B1 (BC-408 material) exposed to (PS) 10  $GeV$  pions beam (LEFT) and (SPS) 100  $GeV$  electrons beam (RIGHT). The signals were fitted with a Languas function.

the hit map reconstructed from experimental data collected at SPS using 350  $GeV$  proton beam centered at the intersection of B9 and B15. As expected, most of the hits are detected in the bars in which the beam is centered on. In order to evaluate the signal shape and its



**Figure 6.13** Left: Prototype layout scheme with beam (red dot) centered in bars B9 and B15. Right: the hit map reconstructed from experimental data collected with the proton beam at SPS, confirming that most of the hits are detected by these 2 bars

dependency on the hit position along the bar, the prototype was moved to the relevant positions beforehand identified to get a meaningful scan of the bar. In both horizontal and vertical bars, the trend of signal amplitudes follows the expected behaviour (exponential-like curve, as shown in fig. 6.14): the longer the distance between the impact point and the SiPM, the lower the signal amplitude.

The light yield of 2 different scintillator materials (EJ-204 and BC-404) operated at similar conditions in the PSD prototype was also measured at SPS by means of a proton beam. As shown in fig. 6.15, there is no evidence of pronounced differences.

**6.1.5.3 Cosmic-rays and radioactive sources** These measurements were mostly performed at the INFN laboratories in Bari and LNGS. The measurements with muons were taken using an external trigger in a “sandwiched” configuration, with a first scintillator above the PSD and a second one underneath (the PSD element is therefore in between). The  $^{90}\text{Sr}$  measurements, on the other hand, could not be done in the same way since most

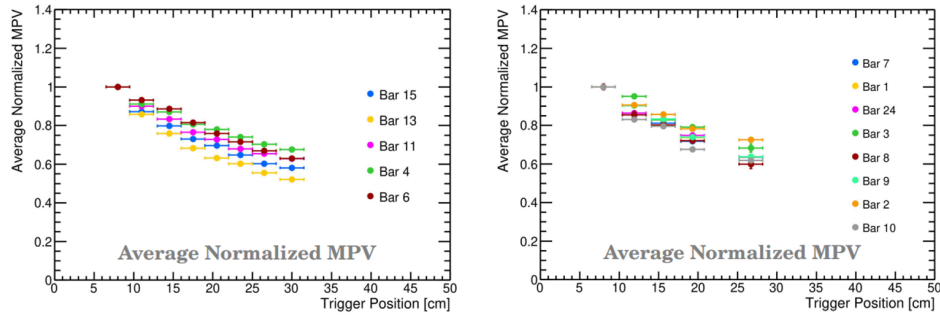


**Figure 6.14** MPV of the charge peak distribution as a function of the distance between the beam and the SiPMs position. The charge has been averaged over the 2 bar channels and normalized to the maximum charge value among all the bars in the same layer, for horizontal bars (left) and vertical bars (right). As expected, the longer the distance between the impact point and the SiPMs, the lower the MPV value (see inline text for more details. (Preliminary result.)

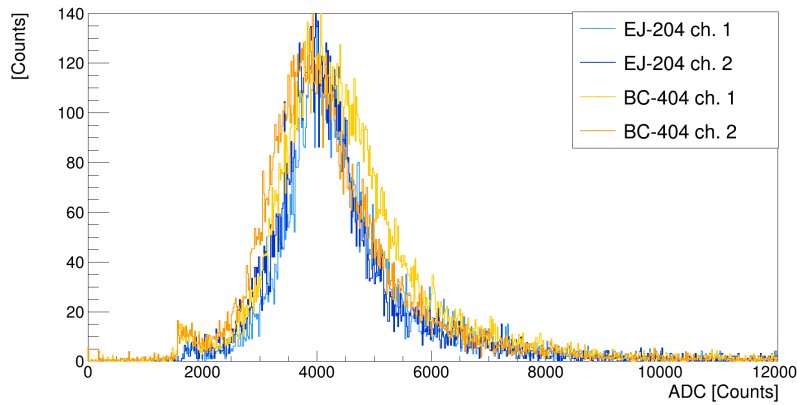


**Figure 6.15** Light yield comparison of BC-404 and EJ-204 scintillator materials, with no evidence of major differences.

of the electrons from the source would stop before reaching the bottom part of the trigger. The solution adopted was to place the source on the element to be tested and the *and-logic* of 2 SiPMs inside the same element was used as trigger. This approach has been adopted to measure the light propagation in the scintillator. A schematic example of these test configurations is reported in fig. 6.16.

Most of the tests performed in Bari on the tiles were carried out using a  $^{90}\text{Sr}$  source with about  $2\text{MBq}$  of intensity, and cosmic-rays. The signals were triggered either in self-trigger mode (choosing a proper threshold) or in *AND* mode (coincidence of 2 or more SiPM signals). The main goal was to study the uniformity response in light collection as a function of the impinging particle positions and the mean acquisition time of the signals (currently ongoing). Many SiPM configurations and wrapping procedures were tested: the best response is obtained with the SiPMs coupled to the lateral side of the tiles.

Figure 6.17 shows the comparison between the measurements obtained in the laboratory (left), using the  $^{90}\text{Sr}$  source in the *AND* trigger logic (2 SiPM coincidence signals), and by



**Figure 6.16** Schematic example of PSD element testing using CR muons (left) or radioactive source (right)

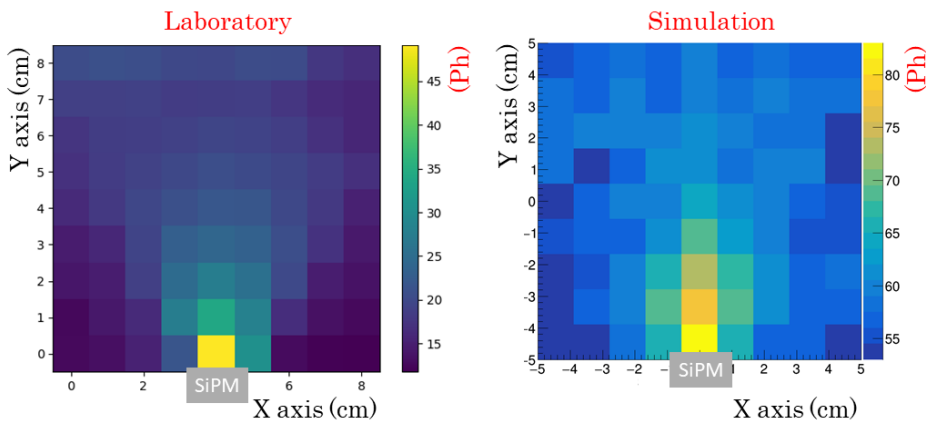


**Figure 6.17** Comparison between data acquired in laboratory and MC simulation. The color plot shows the mean number of photons acquired by the SiPM moving a source of  $^{90}\text{Sr}$  in x and y position by step of 1 cm long.

acquiring the signal at the bottom side, and ca MC simulation (SiPM PDE is not taken into account) based on GEANT4 [15, 16, 17]. The  $^{90}\text{Sr}$  was moved in x and y direction in steps of 1 cm and the acquired signal was processed to obtain the mean number of photons.

The photon distribution is influenced by the position of the MIP on the tile (in this case an electron distribution with the end-point of about  $2\text{MeV}$ ). This kind of study is useful to have a more accurate measurement of the position of the primary particle and can be used also to distinguish, in principle, a single localized impinging particle from a diffuse shower.

The test on the bars were focused on the measurements of the attenuation length, the exported charge distributions from each SiPM in various trigger positions along the bar were fitted with a Landau function. Afterwards, the Most Probable Value (MPV) of each contribution is plotted with respect to the trigger position and normalized to the maximum value, in order to highlight the behaviour of light attenuation along the bar. The tests were performed to a large variety of bars, the results shown in fig. 6.18 are the ones for the 150 cm long bar, 3 cm width and 1 cm thick, the most like the ones going in the full-scale prototype. The exponential fit of these results yields an attenuation length of  $\Lambda = 184 \pm 13$  cm.

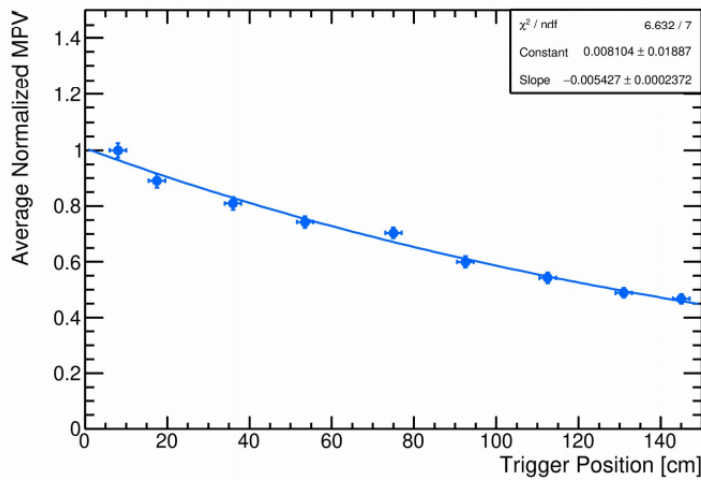


**Figure 6.18** Charge peak fitted as Landau distribution MPV, averaged over the 2 SiPMs and normalized to the maximum value, plotted as a function of the distance from the trigger to the SiPM, together with an exponential fit which yields an attenuation length  $\Lambda = 184 \pm 13$  cm. (Preliminary result.)

## 6.2 PSD Work plan

In the following a list of the main activities foreseen till the end of 2023

- January/August 2022 Studies of the performances of small scale tile and bar prototypes in IHEP and INFN laboratories
- March 2022 Preliminary irradiation testing of Novel Design Laboratory (NDL) SiPMs will be performed in February or March in China Spallation Neutron Source
- March 2022 Test on the first version of  $\beta$ -chip
- March/December 2022 Several Beam Test at CNAO facility in Italy with low energy nuclei to study the effect of signal saturation and fragmentation with different small scale PSD prototypes
- May/September 2022 Design and test of PSD mechanics
- September/October 2022 Test of the first production of FBK SiPMs
- September/October 2022 Assembly of PSD prototype for CERN Beam Test
- October/November 2022 Beam Test at CERN with protons, electrons, muons, ions with an integrated plane of the PSD readout with a non-flight version of the readout system. The goal of this test is to fully characterized the PSD (charge resolution, linearity, efficiency, ...) and to test the synchronous readout with other sub-detector
- January/March 2023 Subsystem Interface and protocol design and test
- March 2023 test with the flight version of  $\beta$ -chip

- September/October 2023 Assembly of PSD prototype for CERN Beam Test
- October/November 2023 Beam Test at CERN with protons, electrons, muons, ions with an engineering model of HERD payload partially equipped with active elements and with a flight version of the readout system. The goal of this test is to fully test the assembled detector.

## REFERENCES

---

- [1] AA Moiseev, JF Ormes, RC Hartman, TE Johnson, JW Mitchell, and DJ Thompson. Observation and simulations of the backplash effects in high-energy gamma-ray telescopes containing a massive calorimeter. *Astroparticle Physics*, 22(3):275–283, 2004.
- [2] Y Yu et al. The plastic scintillator detector for dampe. *Astroparticle Physics*, 94:1–10, 2017.
- [3] Z-L Xu et al. An algorithm to resolve  $\gamma$ -rays from charged cosmic rays with dampe. *Res. Astron. Astrophys.*, 18(3):027, 2018.
- [4] [https://www.hamamatsu.com/resources/pdf/ssd/s14160-1310ps\\_etc\\_kapd1070e.pdf](https://www.hamamatsu.com/resources/pdf/ssd/s14160-1310ps_etc_kapd1070e.pdf).
- [5] Fondazione bruno kessler. <https://www.fbk.eu/en/>.
- [6] P. W. Cattaneo, M. Pullia, M. C. Prata, A. Rappoldi, and M. Rossella. Beam test characterisation of a Plastic Scintillator Prototype for the space-based cosmic ray experiment HERD. *JINST*, 15(07):C07027, 2020.
- [7] PS Marrocchesi, O Adriani, Y Akaike, MG Bagliesi, A Basti, G Bigongiari, S Bonechi, M Bongi, MY Kim, T Lomtadze, et al. Beam test performance of a scintillator-based detector for the charge identification of relativistic ions. *Nuclear Instruments and Methods in Physics Research Section A: Accelerators, Spectrometers, Detectors and Associated Equipment*, 659(1):477–483, 2011.
- [8] Hamamtsu sipm s12572-010c. [https://www.hamamatsu.com/resources/pdf/ssd/s12572-010\\_etc\\_kapd1045e.pdf](https://www.hamamatsu.com/resources/pdf/ssd/s12572-010_etc_kapd1045e.pdf).
- [9] Hamamtsu sipm s12572-050p. <https://ibook.antpedia.com/attachments/product/212/1426215004-7605.pdf>.
- [10] C Altomare, P De La Torre Luque, L Di Venere, P Fusco, F Gargano, F Giordano, P Hu, F Loparco, S Loporchio, MN Mazziotta, et al. Particle identification capability of plastic scintillator tiles equipped with sipms for the high energy cosmic-radiation detection (herd) facility.

- Nuclear Instruments and Methods in Physics Research Section A: Accelerators, Spectrometers, Detectors and Associated Equipment*, 983:164476, 2020.
- [11] C Altomare, P De La Torre Luque, L Di Venere, P Fusco, F Gargano, F Giordano, P Hu, F Loparco, S Loporchio, MN Mazziotta, et al. A full and customizable simulation of a scintillation tile equipped with sipms for plastic scintillator detectors in the next generation of satellite experiments. *Nuclear Instruments and Methods in Physics Research Section A: Accelerators, Spectrometers, Detectors and Associated Equipment*, 982:164479, 2020.
- [12] Caen daq dt5550w board. <https://www.caen.it/products/dt5550w/>.
- [13] Bc-404 scintillator datasheet. <https://www.crystals.saint-gobain.com/sites/imdf.crystals.com/files/documents/bc400-404-408-412-416-data-sheet.pdf>.
- [14] Ej-204 scintillator datasheet. <https://eljentechnology.com/products/plastic-scintillators/ej-200-ej-204-ej-208-ej-212>.
- [15] Sea Agostinelli, John Allison, K al Amako, John Apostolakis, H Araujo, P Arce, M Asai, D Axen, S Banerjee, G 2 Barrand, et al. Geant4—a simulation toolkit. *Nuclear instruments and methods in physics research section A: Accelerators, Spectrometers, Detectors and Associated Equipment*, 506(3):250–303, 2003.
- [16] J Allison, Katsuya Amako, John Apostolakis, Pedro Arce, M Asai, T Aso, E Bagli, A Bagulya, S Banerjee, GJNI Barrand, et al. Recent developments in geant4. *Nuclear Instruments and Methods in Physics Research Section A: Accelerators, Spectrometers, Detectors and Associated Equipment*, 835:186–225, 2016.
- [17] John Allison, Katsuya Amako, JEA Apostolakis, HAAH Araujo, P Arce Dubois, MAAM Asai, GABG Barrand, RACR Capra, SACS Chauvie, RACR Chytracek, et al. Geant4 developments and applications. *IEEE Transactions on nuclear science*, 53(1):270–278, 2006.

# CHAPTER 7

---

## SCD

---

this is the SCD chapter.

### 7.1 baseline design

- functions
- working principles, technical approach, main components
- technical specifications, key performance
- resources requirements, device list and external interface
- key technology, technical readiness level, risk analysis
- product matrix

### 7.2 work plan

- work plan(Covering the next two years (phase B and pre-C in ESA/ECSS)), task list and milestone
- product lists and documentation
- target specifications



# CHAPTER 8

---

## TRD

---

this is the TRD chapter.

### **8.1 baseline design**

- functions
- working principles, technical approach, main components
- technical specifications, key performance
- resources requirements, device list and external interface
- key technology, technical readiness level, risk analysis
- product matrix

### **8.2 work plan**

- work plan(Covering the next two years (phase B and pre-C in ESA/ECSS)), task list and milestone
- product lists and documentation
- target specifications



## CHAPTER 9

---

# GENERAL STRUCTURE AND THERMAL

---

this is the general structure and thermal chapter.

### 9.1 baseline design

- functions
- working principles, technical approach, main components
- technical specifications, key performance
- resources requirements, device list and external interface
- key technology, technical readiness level, risk analysis
- product matrix

### 9.2 work plan

- work plan(Covering the next two years (phase B and pre-C in ESA/ECSS)), task list and milestone
- product lists and documentation
- target specifications



## CHAPTER 10

---

# GENERAL ELECTRONICS AND SOFTWARE

---

this is the general electronics and software chapter.

### 10.1 baseline design

- functions
- working principles, technical approach, main components
- technical specifications, key performance
- resources requirements, device list and external interface
- key technology, technical readiness level, risk analysis
- product matrix

### 10.2 work plan

- work plan(Covering the next two years (phase B and pre-C in ESA/ECSS)), task list and milestone
- product lists and documentation
- target specifications